Journal of Materials Chemistry A

RSC Publishing

PAPER

View Article Online
View Journal | View Issue

Cite this: J. Mater. Chem. A, 2013, 1, 13308

Received 26th July 2013
Accepted 2nd September 2013

DOI: 10.1039/c3ta12914d

www.rsc.org/MaterialsA

Design of water-soluble CdS–titanate–nickel nanocomposites for photocatalytic hydrogen production under sunlight†

Cao-Thang Dinh,[a] Minh-Hao Pham,[a] Freddy Kleitz[b] and Trong-On Do*[a]

We report a highly active and stable nanocomposite photocatalyst for H_2 generation under sunlight which consists of a rational assembly of CdS nanoparticles, Ni clusters, and ultrathin titanate nanodisks, highly dispersed in water.

Since the discovery of photo-induced water splitting on TiO_2 electrodes,[1] the use of semiconductors for photocatalytic H_2 production from water has attracted tremendous interest as it allows for the production of clean and renewable energy directly from solar irradiation.[2] Among various photocatalysts developed so far, metal sulfides have been proven to be good candidates for photocatalytic H_2 production from water containing sacrificial reagents under visible light.[3–14] In particular, CdS has been most frequently investigated, due to its efficient absorption of visible light and sufficient conduction band (CB) potential for reduction of H^+ to H_2.[5–14] However, CdS alone exhibits very low photocatalytic activity due to the quick recombination of photo-induced charge carriers. Good performances were mostly achieved in the presence of noble metal co-catalysts, such as Pt and Pd.[2,5,6] Recently, nickel-based compounds such as cationic nickel, metallic nickel or nickel sulfides have been demonstrated to be effective cocatalysts for H_2 generation.[15–17] The use of earth-abundant and inexpensive nickel based cocatalysts could open up new opportunities in design of efficient photocatalysts for H_2 production.[18]

Among various strategies to improve the photocatalytic activity of CdS, the most efficient method is to promote the charge separation of photogenerated electrons and holes by coupling CdS to other semiconductors with adequate flat band potentials such as TiO_2,[7,8,19] ZnO,[9,20–22] and titanate,[23–25] or coupling CdS to graphene.[10,26–28] In such systems, electrons from the CB of CdS can transfer to other semiconductors or graphene, leading to improved electron–hole separation. It has been suggested that direct interfacial contact between semiconductors is required to obtain good charge transfer between them, and that vectorial electron transfer in multicomponent semiconductor composites, in which electrons are transferred between components in one direction, would significantly enhance the charge separation.[11–13] However, developing such a multicomponent system requires precise control over the position of each component in the composite. Therefore, only a limited number of studies on vectorial electron transfer composite photocatalysts have been reported, with limited control over their structures and costly noble metals usually used as cocatalysts.[11] Furthermore, as photocatalytic H_2 production is performed in aqueous medium, high dispersion of the photocatalysts may enable this process under essentially homogeneous reaction conditions, making the photocatalytic H_2 production more efficient. To the best of our knowledge, such a water-soluble non-noble metal heterogeneous photocatalyst has not been developed yet.

Herein, we report the design of a novel type of non-noble metal nanocomposite (NC) for the photo-production of H_2 under direct sunlight by enhancing both its charge separation and aqueous dispersion. The NCs which are composed of CdS nanoparticles (NPs), Ni clusters, and ultrathin titanate nanodisks (TNDs) are highly dispersed in water (namely, water-soluble CdS–TND–Ni NCs). The use of water-soluble TNDs with negatively charged surface compensated by tetraethylammonium cations (TEA^+–TNDs) is found to be crucial to the construction of highly active CdS–TND–Ni NCs. These TEA^+–TNDs facilitate the design of the NCs in which CdS NPs are in intimate contact with the TNDs and Ni clusters could be selectively located on the surface of TNDs as cocatalysts. Thus, in these NCs, the generated electrons in CdS under visible light illumination can be vectorially transferred to the Ni clusters through TNDs. Consequently, charge separation in the NCs is greatly enhanced as the electrons are now separated from holes over three different components. We found that, under direct sunlight illumination, the NCs could generate H_2 from ethanol–water solution with the rate as high as 3.182 mmol h^{-1} (31.820 mmol g^{-1} h^{-1}), representing one of the most highly active metal sulphide photocatalysts in the absence of noble metal cocatalysts.[2]

[a]Department of Chemical Engineering and Centre de Catalyse et Chimie Verte, Laval University, Quebec, G1V 0A6, Canada

[b]Department of Chemistry and Centre de Recherche sur les Matériaux Avancés, Laval University, Quebec, G1V 0A6, Canada. E-mail: trong-on.do@gch.ulaval.ca

† Electronic supplementary information (ESI) available: Additional figures and experimental procedures. See DOI: 10.1039/c3ta12914d

The water-soluble CdS–TND–Ni NC photocatalysts were synthesized by a three-step process as illustrated in Scheme S1.† First, water-soluble TNDs were synthesized. Next, CdS NPs were intimately combined to TNDs forming water-soluble CdS–TND hybrids. Finally, Ni clusters were selectively deposited on the surface of TNDs in CdS–TND hybrids by photodeposition. The preparation of water-soluble TNDs (tetraethylammonium cation exchange TNDs (TEA^+–TND)) was performed by the approach described in our previous work.[29] Transmission electron microscopy (TEM) (Fig. S1†) reveals that the obtained TNDs are uniform in size with a mean particle diameter of 20 nm and a thickness of 0.75 nm.

The most important step in designing CdS–TND–Ni NCs is the synthesis of water-soluble CdS–TND hybrids. These hybrids were prepared from TNDs using a multi-cycle pathway as depicted in Fig. 1. Each cycle consists of (i) exchanging the TEA^+–TND with Cd^{2+} to form precipitated Cd^{2+}–TND and (ii) reacting Cd^+–TND with TEA^+ cations and thiourea at 70 °C to form a TEA^+–CdS–TND hybrid dispersed in water. The key point in this strategy is that once the Cd^{2+} cations located between the TND layers are converted to CdS NPs attached to TNDs by reacting with S^{2-}, the negative charge of the TND surface is again compensated by TEA^+ producing a TEA^+–CdS–TND hybrid which is soluble in water. Hence, the TEA^+–CdS–TND is ready for another cation exchange with Cd^{2+} starting a new cycle. As a result, by repeating this cycle, we can both increase the content of CdS and tune the morphology of the resulting hybrid, and consequently, hybrid systems with desired morphology and composition can be obtained.

Although several methods have been used for the synthesis of CdS–TiO_2 and CdS–titanate hybrids such as co-precipitation,[30] photodeposition,[31,32] chemical bath deposition,[33,34] or layer-by-layer deposition,[35] our approach toward CdS–titanate hybrids is different. Here, by using water-soluble TNDs, we are able to design CdS–TND hybrid colloids stabilized by tetraethylammonium (TEA) cations, as confirmed by FTIR (Fig. S2†), which are highly dispersed in water under static conditions (Fig. S3†). The CdS–TND solution exhibited a negative zeta potential of −46 mV (Fig. S4†), indicating a high stability of this colloidal solution. It is also noted that, under similar synthesis conditions, but in the absence of TNDs, the precipitation of CdS NPs in water was observed. This water-soluble property of CdS–TND hybrids, which has not been previously reported, may facilitate the photocatalytic H_2 production which is usually performed under aqueous medium. In addition, as the CdS NPs are formed between the TND layers, the interfacial contact between CdS and TNDs is greatly enhanced which is important for the electron transfer between the two semiconductors.

Fig. 2a and b show TEM images at different magnifications of the CdS–TND hybrids obtained after 5 cycles of CdS growth. It can be observed from Fig. 2a that the resulting colloidal hybrids are uniform in size with a mean particle diameter of 40 nm. The high-resolution TEM images (Fig. 2c and d and S5†) reveal that each colloid consists of both TNDs and CdS NPs (see the schematic illustration of the CdS–TND hybrid structure in Fig. S6†). It should be mentioned that it is difficult to observe the TNDs in the CdS–TND hybrids when they lie perpendicular to the electron beam due to their ultrathin structure. Only TNDs which are oriented parallel to the direction of the electron beam could be clearly visualized. Fig. 2d shows the structure of individual CdS NPs in the CdS–TND hybrid with an average crystallite size of 5–7 nm. The lattice fringes of the CdS NPs with a *d*-spacing of 0.335 nm can be assigned to the (111) lattice plane of the cubic CdS.[10] Fig. 2d and S5† also show the presence of intimate contact between CdS and TNDs. This close contact between the two semiconductors may enhance the charge transfer between them, improving the charge separation and thus the photocatalytic efficiency. Elemental mapping of an individual CdS–TND hybrid colloid particle (Fig. 2, lower panel) clearly demonstrates a homogeneous distribution of Cd, S, Ti, and O elements over the entire hybrid particle. This result further confirms that TNDs and CdS nanocrystals are uniformly intercalated together in the colloidal hybrid structure.

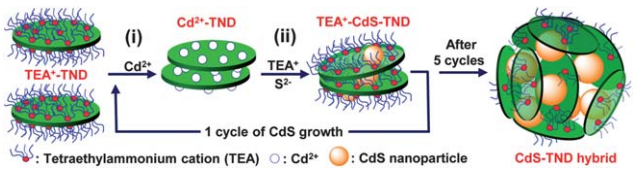

Fig. 1 Illustration of the synthesis of the water-soluble CdS–TND hybrid colloids. (i) Exchanging the TEA^+–TND with Cd^{2+} to form Cd^{2+}–TND; (ii) reacting Cd^{2+}–TND with TEA^+ and thiourea at 70 °C to form TEA^+–CdS–TND hybrids.

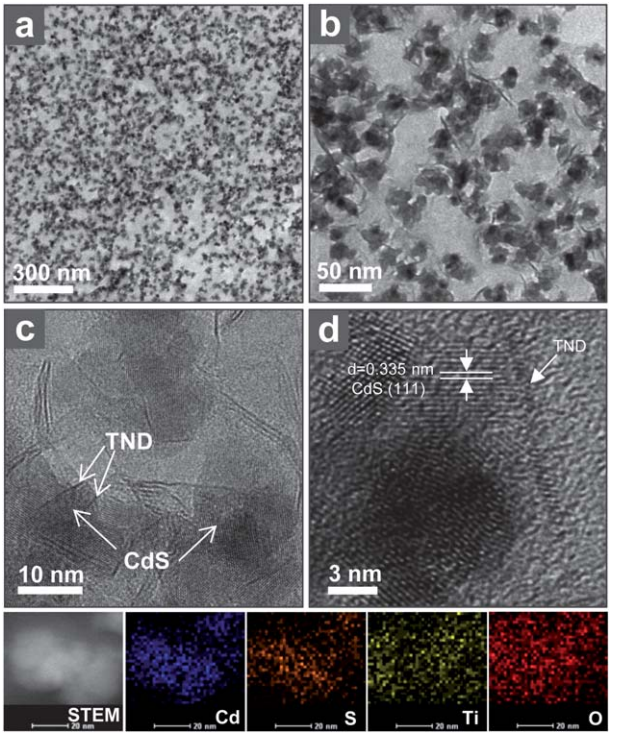

Fig. 2 TEM images (a and b), HRTEM images (c and d) with different magnifications, and EDX elemental mapping data (lower panel) of CdS–TND hybrids obtained by 5 cycles of CdS growth. TEM images show the high dispersion and uniform size of CdS–TND hybrids. HRTEM images confirm the presence and the intimate contact of CdS NPs and TNDs in each CdS–TND hybrid colloid.

The crystallographic structure of CdS in the CdS–TND hybrids was also revealed by powder X-ray diffraction (XRD). As shown in Fig. S7,† all of the main diffraction peaks of the CdS in the CdS–TND hybrids can be indexed to cubic CdS (JSPDS card no. 10-0454). The presence of two shoulder peaks located at a 2-θ of 25.02° and 28.02° suggests the occurrence of hexagonal CdS in the obtained CdS–TND hybrid colloids. The composition of the CdS–TND hybrids was determined using the EDX technique as shown in Fig. S8.† The result indicates a Cd : Ti molar ratio of 1.14 in the obtained hybrid sample. The amount of TEA in the CdS–TND hybrid estimated by TGA is 8.1 wt%. Fig. S9† shows the diffuse-reflectance UV-vis spectra of the CdS–TND hybrids, in comparison to the TNDs. It can be observed that the TNDs only adsorb light with wavelength lower than 320 nm. In contrast, the CdS–TND hybrids exhibit a strong absorption in the visible region indicating the excellent visible light harvesting ability of this hybrid system.

Ni clusters were selectively deposited as cocatalysts on the surface of TNDs in the CdS–TND hybrids using photodeposition. Typically, $Ni(NO_3)_2$ was added to the solution containing CdS–TND hybrids (Ni : Ti molar ratio of 1 : 20). Because the surface of TNDs is negatively charged, positively charged Ni^{2+} is selectively adsorbed on the TND surface through a cation exchange process with TEA^+, resulting in CdS–TND–Ni^{2+}. As only a small portion of TEA^+ (~20% mol) on the TND surface was replaced by Ni^{2+}, the resulted CdS–TND–Ni^{2+} is still highly dispersed in the solution. CdS–TND–Ni^{2+} was then precipitated from the solution by adding an excess amount of acetone to remove any possible non-adsorbed Ni^{2+}. The obtained precipitate was washed with acetone to remove the physically adsorbed Ni^{2+} on the CdS surface to ensure that only exchanged Ni^{2+} cations on the surface of TNDs were retained. Note that due to the high solubility of NiS compared to that of CdS,[36] cation exchange between Ni^{2+} and CdS to form NiS is not favored. The S 2p X-ray photoelectron spectroscopy (XPS) spectrum of CdS–TND–Ni^{2+} (Fig. S10†) also confirmed the absence of NiS in the resulting hybrid. The CdS–TND–Ni^{2+} was then re-dispersed in an aqueous ethanol solution 20% (v/v) and illuminated with visible light for 2 h to reduce Ni^{2+} into metallic Ni clusters (see the ESI† for details).

Elemental analysis by atomic absorption spectroscopy reveals a 1.2 wt% of Ni in the CdS–TND–Ni NCs. However, attempts to identify Ni clusters in CdS–TND–Ni NCs using electron microscopy resulted in ambiguous images which may be due to the ultra-small size and high dispersion of Ni clusters. This could be due to the strong interaction between Ni^{2+} and TNDs and a low contrast of Ni species in CdS–TNDs. Thus, XPS was used to monitor the change in chemical states of Ni^{2+} after photo-reduction. Fig. S11† shows the high-resolution XPS spectrum of Ni 2p of the CdS–TND–Ni NCs in comparison to that of two reference samples, *e.g.*, CdS–Ni and metallic Ni NPs prepared by chemical reduction using $NaBH_4$. As seen in Fig. S11,† the Ni $2p_{3/2}$ XPS spectrum of the Ni NPs reference sample shows two peaks at 852.4 and 855.3 eV, corresponding to the presence of metallic Ni and NiO, respectively.[37,38] The presence of NiO in the reference sample could be due to the partial oxidation of the metallic Ni NP surface upon contact with air. A similar result was observed in the Ni $2p_{3/2}$ XPS spectrum of the CdS–Ni sample. Surprisingly, the XPS spectrum of Ni $2p_{3/2}$ of the CdS–TND–Ni NC sample exhibits only one peak at a binding energy of 855.3 eV which is characteristic of NiO. The absence of metallic Ni in the CdS–TND–Ni sample could be due to the instability of metallic Ni clusters in air. These metallic Ni clusters formed by reducing Ni^{2+} under illumination are easily oxidized yielding NiO in air. The formation of metallic Ni clusters on the surface of TNDs in CdS–TND hybrids can be described as follows: under visible light illumination, the generated electrons in the CB of CdS (−0.7 V *vs.* SHE) can be transferred to the CB of TNDs (−0.38 V *vs.* SHE).[39,40] Because the potential of Ni^{2+}/Ni (−0.23 V *vs.* SHE, pH = 0) is lower than the CB level of TNDs,[41,42] the electrons from the CB of TNDs can effectively reduce Ni^{2+} species adsorbed on their surface forming metallic Ni clusters (Fig. S12†).

The photocatalytic H_2 generation activity of the samples was first evaluated under visible light illumination for the purpose of comparison. Fig. 3 shows the photocatalytic H_2-production rates of a series of samples from an aqueous solution containing 20% ethanol (v/v) under visible light illumination: CdS–TND–Ni NCs, CdS–TNDs and CdS alone (obtained under the same synthetic conditions as those of CdS–TND hybrids, except that no TNDs were added, see ESI and Fig. S13†). In addition, photocatalytic activities of CdS–Ni (1.2 wt% of Ni), CdS–Pt (1.2 wt% of Pt) and a mixture of CdS NPs and TND–Ni^{2+} in which Ni^{2+} is adsorbed on the TND surface, were also evaluated. As seen in Fig. 3, CdS alone shows very low H_2 generation rates (0.098 mmol h^{-1} g^{-1}) which is mainly caused by rapid recombination of photogenerated electrons and holes and the lack of H_2 evolution sites.[5,6] Coupling CdS to TNDs improves the H_2 production rate of CdS. As shown in Fig. 3, CdS–TND hybrids exhibit a H_2 production rate of 0.142 mmol g^{-1} h^{-1} which is about 1.4 times higher than that of CdS alone. It should be noted that the content of CdS in CdS–TND hybrids is 67 wt%. Thus, if the rate calculation is based on the amount of CdS, the H_2 production over CdS–TND hybrids would be higher. Interestingly, the introduction of a Ni cocatalyst resulted in a

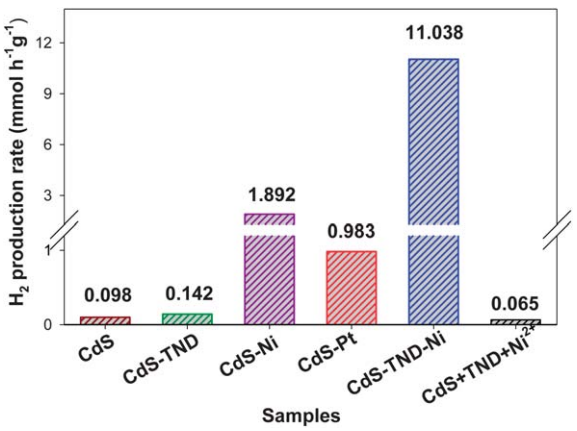

Fig. 3 Comparison of the activity of different photocatalysts in the photocatalytic production of H_2 from an ethanol–water mixture under visible light illumination.

significant improvement in the photocatalytic H_2 production activity for both CdS and CdS–TND hybrids. The H_2 production rate of CdS–Ni (1.892 mmol g^{-1} h^{-1}) is even higher than that of a reference CdS–Pt (0.983 mmol g^{-1} h^{-1}) using noble metal Pt as the cocatalyst (Fig. 3). This confirms that Ni can act as an excellent cocatalyst for the photocatalytic H_2 generation from ethanol–water solution. As shown in Fig. 3, with Ni as the cocatalyst, CdS–Ni exhibits a 19-fold higher photocatalytic activity compared to that of CdS alone. More impressively, in the presence of Ni clusters on the TND surface, CdS–TND–Ni NCs show a significantly increased photocatalytic activity, by a factor of 77, as compared to CdS–TND hybrids. The apparent quantum yield was measured to be 21% at 420 nm, which is among the highest values reported for noble metal-free CdS-based photocatalysts studied under similar conditions.[2] Note that a simple mixture of CdS NPs and TND–Ni^{2+} with a similar composition to that of CdS–TND–Ni NCs exhibited a very low H_2 production rate. Thus, these results reveal a cooperative effect of TNDs and Ni for the enhancement of H_2 production using CdS. In particular, intimate contact and proper organization of the three components in the NCs are required to achieve high photocatalytic performance.

Although there are numerous reports about CdS-based photocatalysts with different nanostructures and high H_2 production rate under visible light irradiation using different sacrificial agents such as lactic acid, methanol, ethanol, propanol and Na_2S + Na_2SO_3, most of them are achieved with a Pt cocatalyst.[2] For example, Amirav *et al.*[43] reported a nano-heterostructure composed of a Pt-tipped CdS rod with an embedded CdSe seed which exhibited a H_2 generation rate of 40 mmol g^{-1} h^{-1} under visible light illumination, and an apparent quantum yield of 20% at 420 nm using methanol as the sacrificial agent. Li *et al.*[10] reported the H_2 gas evolved at a rate of 56 mmol g^{-1} h^{-1} corresponding to an apparent quantum yield of 22.5% at 420 nm for the samples of Pt-loaded CdS–cluster-decorated graphene nanosheets using lactic acid as the sacrificial agent. Recently, Wang *et al.*[22] reported a H_2 generation rate of 19.2 mmol g^{-1} h^{-1} under visible light illumination for the sample of the Pt-loaded ZnO–CdS@Cd heterostructure using Na_2S + Na_2SO_3 as the sacrificial agent. Without noble–metal cocatalysts, however, most of the reported CdS-based photocatalysts exhibit H_2 generation rates of 0.070–1.600 mmol g^{-1} h^{-1} (Table S1†) using either ethanol or Na_2S + Na_2SO_3 as the sacrificial agent, which are several times lower than the observed H_2 generation rate of the present CdS–TND–Ni NC photocatalyst (11.038 mmol g^{-1} h^{-1}). The high H_2 production activity of CdS–TND–Ni NCs under visible light can be due to Ni clusters highly dispersed on the surface of TNDs. Under visible light irradiation, the generated electrons from the CB of CdS can effectively be injected into the CB of TNDs due to an intimate interaction between the two semiconductors (see the scheme in Fig. 4). Ni clusters deposited on the surface of TNDs can cap the electrons from TNDs and act as active sites for H_2 evolution. Thus, the electrons and holes in the NCs are separated from each other over three different components, leading to effective prolongation of the charge carrier lifetime and enlargement of the reaction space, and consequently, the improvement of the

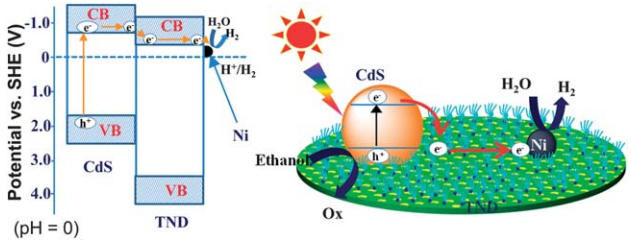

Fig. 4 Schematic illustration of the charge transfer in CdS–TND–Ni NCs in the photocatalytic H_2 production from a water–ethanol mixture under visible light. To simplify, only one particle of each component is shown, although a NC colloid is composed of several CdS NPs, TNDs and Ni clusters.

photocatalytic H_2 production. In addition, the presence of TEA on the surface of TNDs makes the NCs highly dispersed in the ethanol–water mixture, but does not affect the surface of CdS NPs and Ni clusters. Thus, the reactants (water and ethanol) are free to access the active sites on the CdS and Ni surface with high diffusion rate. Therefore, the photocatalytic rate is significantly enhanced.

The stability of the CdS–Ni and CdS–TND–Ni was studied by performing recycle experiments under the same conditions. After 5 cycles, the photocatalytic H_2 production rate of CdS–Ni photocatalysts decreased gradually and remained only 52% of the initial rate (Fig. 5). In contrast, the CdS–TND–Ni NCs showed no photocatalytic activity loss, indicating the high stability of this photocatalyst for the H_2 generation. It is important to note that metal sulfide photocatalysts are usually unstable during photocatalytic reaction due to (i) reduction of metal cations in metal sulfides by generated electrons; (ii) oxidation of S^{2-} by generated holes; and (iii) detachment of metallic NP cocatalysts from the metal sulfide surface due to the photooxidation of metal particles.[5,6,43–45] In the case of CdS–TND–Ni NCs, adequate electron transfer from the CB of CdS to that of TNDs originated from the intimate interactions between CdS and TNDs is beneficial for preventing the reduction of Cd^{2+}. In addition, the high dispersion of the photocatalysts in the reacting medium favors the accessibility of the sacrificial agent (ethanol) to the surface of CdS, leading to the suppression of the oxidation of S^{2-} on CdS. Furthermore, in the CdS–TND–Ni NCs,

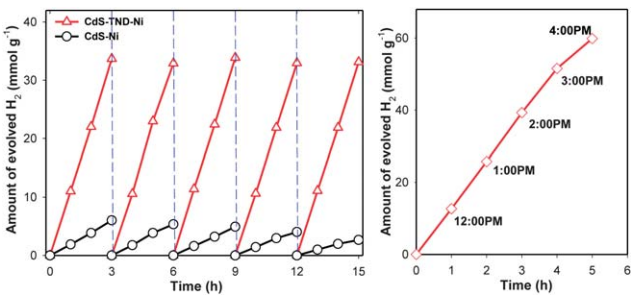

Fig. 5 H_2 production from CdS–TND–Ni and CdS–Ni photocatalysts monitored over 15 h. Every 3 h, the reaction system is bubbled with N_2 for 15 min to remove the H_2 inside (left). H_2 production rate from ethanol–water solution with CdS–TND–Ni NCs under natural sunlight (May 7, 2013; at Laval University, QC, Canada) (right).

only CdS can generate holes in the valence band (VB) under visible light illumination. These holes in the VB of CdS (+1.7 V *vs.* SHE) cannot be transferred to the VB of TNDs (+3.4 V *vs.* SHE).[39,40] Thus, Ni clusters are unlikely to be directly oxidized by holes on CdS NPs as they are only located on the surface of TNDs. This is different from the oxidation of nickel species on the surface of semiconductors when they are directly contacted with photogenerated holes.[46] Taking into account these unique features, it is not surprising that the CdS–TND–Ni NCs exhibit not only high activity, but also high stability in the photocatalytic generation of H_2. We observed that the CdS–TND–Ni photocatalyst was still highly dispersed in the solution even after 5 cycles of photocatalytic reaction. The TGA analysis of the samples before and after 5 cycles of reaction (Fig. S14†) showed identical curves, indicating that the TEA cations on the surface of TNDs are not decomposed during the photocatalytic process. In addition, TEM images (Fig. S15†) indicate that the morphology of the CdS–TND–Ni NCs is preserved after the 5 cycles.

Natural sunlight was used to evaluate the potential application of the CdS–TND–Ni NCs in H_2 production. As shown in Fig. 5 (right), H_2 was readily produced from aqueous ethanol solution containing NC photocatalysts under natural sunlight between 11:00 am and 4:00 pm on May 7, 2013 (Quebec city, QC). Impressively, the NCs could generate H_2 with the average rate as high as 1.232 mmol h^{-1} (12.326 mmol g^{-1} h^{-1}) over an irradiation area of 125 cm^2, which is even higher than that measured under visible light in the laboratory. Moreover, due to the high dispersion of CdS–TND–Ni NCs in ethanol–water solution, the H_2 generation rate can be further increased simply by increasing the irradiation area. For example, with the same amount of photocatalyst (100 mg) and ethanol–water solution (500 ml), when the irradiation area was 4 times increased, a H_2 generation rate up to 3.182 mmol h^{-1} (31.820 mmol g^{-1} h^{-1}) was obtained under direct sunlight illumination. These results combined with the high stability of CdS–TND–Ni NCs prove the great potential of practical application of the water-soluble CdS–TND–Ni NCs for H_2 production under sunlight. In this case, ethanol was used as the sacrificial agent; however, other renewable biomass derivatives such as glycerol can also be used as sacrificial agents to make this strategy feasible.

In summary, we have designed a novel type of NC photocatalyst for the production of H_2 under sunlight irradiation, consisting of CdS NPs, TNDs, and Ni clusters by using water-soluble TNDs with negatively charged surface compensated by TEA^+ cations. This design has enhanced significantly the electron–hole separation in NC photocatalysts by combining CdS, TNDs, and Ni in such a way that a vectorial electron transfer from CdS to TNDs and then to Ni is enabled. Moreover, the NCs are highly dispersed in water medium. Thus, the obtained NCs show high stability and the highest photocatalytic activity among all of the non-noble metal sulphide-based catalysts for the H_2 generation under visible light, and can thus provide viable solutions for the development of practical photocatalysts for H_2 production under sunlight. We also believe that our design can be extended to other metal sulfide-based NCs, and thus could be applied to produce high performance NCs for applications beyond photocatalysis.

Acknowledgements

This work was supported by the NSERC (Canada) and FQRNT (Province of Quebec). The authors thank Yongbeom Seo and Prof. Ryong Ryoo (KAIST, Korea) for the access to high-resolution TEM microscopy data.

Notes and references

1 A. Fujishima and K. Honda, *Nature*, 1972, **238**, 37.
2 X. B. Chen, S. H. Shen, L. J. Guo and S. S. Mao, *Chem. Rev.*, 2010, **110**, 6503.
3 I. Tsuji, H. Kato, H. Kobayashi and A. Kudo, *J. Am. Chem. Soc.*, 2004, **126**, 13406.
4 J. Zhang, J. Yu, Y. Zhang, Q. Li and J. R. Gong, *Nano Lett.*, 2011, **11**, 4774.
5 N. Bao, L. Shen, T. Takata and K. Domen, *Chem. Mater.*, 2008, **20**, 110.
6 G. Ma, H. Yan, J. Shi, X. Zong, Z. Lei and C. Li, *J. Catal.*, 2008, **260**, 134.
7 S. C. Hayden, N. K. Allam and M. A. El-Sayed, *J. Am. Chem. Soc.*, 2010, **132**, 14406.
8 J. Ryu, S. H. Lee, D. H. Nam and C. B. Park, *Adv. Mater.*, 2011, **23**, 1883.
9 X. Wang, G. Liu, Z. Chen, F. Li, L. Wang, G. Lu and H. Cheng, *Chem. Commun.*, 2009, 3452.
10 Q. Li, B. Guo, J. Yu, J. Ran, B. Zhang, H. Yan and J. R. Gong, *J. Am. Chem. Soc.*, 2011, **133**, 10878.
11 H. Park, W. Choi and M. R. Hoffmann, *J. Mater. Chem.*, 2008, **18**, 2379.
12 I. V. Lightcap, T. H. Kosel and P. V. Kamat, *Nano Lett.*, 2010, **10**, 577.
13 A. Mukherji, B. Seger, G. Q. Lu and L. Wang, *ACS Nano*, 2011, **5**, 3483.
14 P. D. Tran, L. H. Wong, J. Barber and J. S. C. Loo, *Energy Environ. Sci.*, 2012, **5**, 5902.
15 Z. Han, F. Qiu, R. Eisenberg, P. L. Holland and T. D. Krauss, *Science*, 2012, **338**, 1321.
16 W. Wang, S. Liu, L. Nie, B. Cheng and J. Yu, *Phys. Chem. Chem. Phys.*, 2013, **15**, 12033.
17 Y. P. Yuan, S. W. Cao, L. S. Yin, L. Xu and C. Xue, *Int. J. Hydrogen Energy*, 2013, **38**, 7218.
18 G. Wang and Y. Li, *ChemCatChem*, 2013, **5**, 1294.
19 H. Wang, G. Wang, Y. Ling, M. Lepert, C. Wang, J. Z. Zhang and Y. Li, *Nanoscale*, 2012, **4**, 1463.
20 T. Peng, K. Dai, H. Yi, D. Ke, P. Cai and L. Zan, *Chem. Phys. Lett.*, 2008, **460**, 216.
21 X. Wang, G. Liu, G. Lu and H. Cheng, *Int. J. Hydrogen Energy*, 2010, **35**, 8199.
22 X. Wang, G. Liu, L. Wang, Z. G. Chen, G. Q. M. Lu and H. M. Cheng, *Adv. Energy Mater.*, 2012, **2**, 42.
23 H. N. Kim, T. W. Kim, I. Y. Kim and S. J. Hwang, *Adv. Funct. Mater.*, 2011, **21**, 3111.
24 Y. Zhang, Y. Tang, X. Liu, Z. Dong, H. H. Hng, Z. Chen, T. C. Sum and X. Chen, *Small*, 2013, **9**, 996.
25 Y. Chen, L. Wang, G. M. Lu, X. Yao and L. Guo, *J. Mater. Chem.*, 2011, **21**, 5134.

26 A. Ye, W. Fan, Q. Zhang, W. Deng and Y. Wang, *Catal. Sci. Technol.*, 2012, **2**, 969.
27 L. Jia, D. H. Wang, Y. X. Huang, A. W. Xu and H. Q. Yu, *J. Phys. Chem. C*, 2011, **115**, 11466.
28 P. Gao, J. Liu, S. Lee, T. Zhang and D. D. Sun, *J. Mater. Chem.*, 2012, **22**, 2292.
29 C. T. Dinh, Y. Seo, T. D. Nguyen, F. Kleitz and T. O. Do, *Angew. Chem., Int. Ed.*, 2012, **51**, 6608.
30 Y. Bessekhouad, D. Robert and J. V. Weber, *J. Photochem. Photobiol., A*, 2004, **163**, 569.
31 H. Tada, M. Fujishima and H. Kobayashi, *Chem. Soc. Rev.*, 2011, **40**, 4232.
32 M. Fujii, K. Nagasuna, M. Fujishima, T. Akita and H. Tada, *J. Phys. Chem. C*, 2009, **113**, 16711.
33 Q. Shen, J. Kobayashi, L. J. Diguna and T. Toyoda, *J. Appl. Phys.*, 2008, **103**, 84304.
34 S. Gorer and G. Hodes, *J. Phys. Chem.*, 1994, **98**, 5338.
35 D. R. Baker and P. V. Kamat, *Adv. Funct. Mater.*, 2009, **19**, 805.
36 J. R. Goates, M. B. Gordon and N. D. Faux, *J. Am. Chem. Soc.*, 1952, **74**, 835.
37 *Handbook of X-ray Photoelectron Spectroscopy*, ed. J. F. Moulder, W. F. Stickle, P. E. Sobol, K. D. Bomben and J. Chastain, Physical Electronics, Inc., Eden Prairie, MN, 1992.
38 M. C. Biesinger, B. P. Payne, L. W. M. Lau, A. Gerson and R. S. C. Smart, *Surf. Interface Anal.*, 2009, **41**, 324.
39 J. Ran, J. Yu and M. Jaroniec, *Green Chem.*, 2011, **13**, 2708.
40 N. Sakai, Y. Ebina, K. Takada and T. Sasaki, *J. Am. Chem. Soc.*, 2004, **126**, 5851.
41 J. G. Yu, Y. Hai and B. Cheng, *J. Phys. Chem. C*, 2011, **115**, 4953.
42 *Standard Potentials in Aqueous Solution*, ed. A. J. Bard, R. Parsons and J. Jordan, Marcel Dekker, New York, 1985.
43 L. Amirav and A. P. Alivisatos, *J. Phys. Chem. Lett.*, 2010, **1**, 1051.
44 K. Domen, J. N. Kondo, M. Hara and T. Takata, *Bull. Chem. Soc. Jpn.*, 2000, **73**, 1307.
45 J. Zhang, J. Yu, M. Jaroniec and J. R. Gong, *Nano Lett.*, 2012, **12**, 4584.
46 G. Wang, Y. Ling, X. Lu, T. Zhai, F. Qian, Y. Tong and Y. Li, *Nanoscale*, 2013, **5**, 4129.

Supporting Information

Design of Water-soluble CdS-Titanate-Nickel Nanocomposites for Photocatalytic Hydrogen Production under sunlight

Cao-Thang Dinh,[†] Minh-Hao Pham,[†] Freddy Kleitz,[§] and Trong-On Do*[†]

[†] Department of Chemical Engineering and Centre de Catalyse et Chimie Verte (C3V), Laval University, Quebec, G1V 0A6, Canada

[§] Department of Chemistry and Centre de Recherche sur les Matériaux Avancés (CERMA), Laval University, Quebec, G1V 0A6, Canada

Corresponding Author : trong-on.do@gch.ulaval.ca

Chemicals. All chemicals were used as received; Titanium butoxide (TB), benzyl alcohol (BA), oleylamine (OM), benzyl ether, tetraethylammonium (TEA) hydroxide, nickel nitrate, cadmium nitrate, thiourea, chloroplatinic acid, were purchased form Aldrich. Absolute ethanol, acetone, and toluene solvents were of analytical grade and were also purchased form Aldrich.

Synthesis of titanate nanodisks. In a typical synthesis, 2g of TB, 12 g of OM, 12g of BA (OM:BA weight ratio of 1:1), and 30g of benzyl ether were added to a 100-mL round-bottom flask. The reaction mixture was heated to 190 ^{o}C at the heating rate 5 ^{o}C/min under nitrogen flow. After 20 h, the reaction was stopped and cooled down to room temperature. After addition of excess absolute ethanol, the TNDs were obtained by centrifugation. The obtained nanodisks were then re-dispersed in toluene and re-precipitated with ethanol. This process was repeated three times to remove the un-reacted reagents.

Tetraethylammonium-exchanged titanate nanodisks. The as-synthesized TNDs were treated with tetraethylammonium hydroxide to obtain water-soluble TEA-TNDs. Typically, 5 mmol of as-synthesized TNDs (according to Ti atom) were dispersed in a mixture of TEAOH (15 mmol), ethanol (15 ml) and water (15 ml). The mixture was stirred overnight at room temperature. An excess of acetone was added to the obtained clear solution to precipitate TNDs. The precipitate was then washed several times with acetone and finally re-dispersed in 10 ml of water.

Synthesis of CdS-TND hybrids. The CdS-TND hybrids were synthesized using a multi-cycle pathway (Figure 1). In the first cycle, Cd^{2+} cations-exchanged TNDs were prepared. Accordingly, the TEA-TNDs dispersed in water were gradually added to a solution containing Cd^{2+} cations (Cd:Ti atomic ratio of 1:2) under stirring. The resulting Cd^{2+}-TND precipitate was then washed several times with water to remove un-exchanged Cd^{2+} cations. To obtain the CdS-TND hybrid, Cd^{2+}-TNDs was then dispersed in water. To this mixture was added a solution containing both TEAOH and thiourea (TEAOH : thiourea : Cd^{2+} molar ratio of 1:1:0.3). Next, the obtained mixture was heated to 70^{o}C. At this temperature, S^{2-} ions are released by the alkaline hydrolysis of thiourea and reacted with Cd^{2+} yielding CdS nanocrystals. After 1 hour of heating, a yellow transparent solution was formed indicative of the formation of the CdS-TND hybrids. To this clear solution acetone was added in excess to precipitate CdS-TNDs. The yellow precipitate was then washed several times with acetone and finally re-dispersed in water for a subsequent CdS growth cycle. To start the second CdS growth cycle, the CdS-TND hybrids obtained in the previous cycle was used as precursor instead of TEA-TNDs. The following steps were similar to those of the previous cycle. This CdS growth cycle was repeated 5 times to obtain the final TND-CdS hybrid colloids. The obtained CdS-TND hybrids were dispersed in water with the concentration of 10 mg/cm^3.

Synthesis of CdS-TND-Ni nanocomposites. To the CdS-TND hybrid solution was added a solution of $Ni(NO_3)_2$ (Ni^{2+}:Ti molar ratio of 1:20). The mixture was then stirred for 1 hour. During this process, Ni^{2+} was adsorbed on the surface of TNDs through cation exchange process with TEA^+, resulting in CdS-TND-Ni^{2+}. The obtained CdS-TND-Ni^2 was then precipitated from the solution by adding an excess amount of acetone to remove any possible non-exchanged Ni^{2+}. The obtained precipitate was washed with acetone to remove the physically adsorbed Ni^{2+} on the CdS surface to ensure that Ni^{2+} only appeared on the surface of TNDs before being reduced. The CdS-TND-Ni^{2+} was then re-dispersed in an aqueous ethanol solution 20% (v/v) in a gas-tight reaction cell. The solution was evacuated and purged with nitrogen for 10 minutes to completely remove the dissolved oxygen. Finally, the solution was illuminated for 2 hours by a 300W Xe arc lamp equipped with an UV-cutoff filter (≥420 nm). The obtained CdS-TND-Ni NC solution was kept under nitrogen for photocatalytic hydrogen generation test.

Synthesis of CdS nanoparticles. Pure CdS nanoparticles were prepared in the similar conditions to those of the CdS-TND hybrids, but in the absence of TNDs. A mixture of TEAOH and thiourea was added to the solution containing Cd^{2+} cations. The mixture was then heated to 70°C for 1 hour. The resulting precipitate was then washed several times with water and dried at 70°C for 5 hours.

Characterization. Transmission electron microscopy (TEM) images of the samples were obtained on a JOEL JEM 1230 operated at 120kV. High resolution TEM (HRTEM) images were performed on Philips G2 F30 Tecnai instrument operated at 300kV. Powder X-ray diffraction (XRD) patterns of the samples were obtained on a Bruker SMART APEXII X-ray diffractometer equipped with a Cu Kα radiation source (λ=1.5418 Å). Thermal analyses of the samples were carried out at a heating rate of 10 °C/min under a nitrogen flow up to 700 °C using a Perkin-Elmer TGA thermogravimetric analyzer. Zeta potential measurements were performed with a Zetasizer Nano ZS in water at 25 ^{o}C. X-ray photoelectron spectroscopy (XPS) measurements carried out in an ion-pumped chamber (evacuated to 10-9 Torr) of a photoelectron spectrometer (Kratos Axis-Ultra) equipped with a focused X-ray source (Al Kα, hv = 1486.6 eV). The UV-vis spectra were recorded on a Cary 300 Bio UV-visible spectrophotometer. Fourier transform infrared (FTIR) absorption spectra were measured with a FTS 45 infrared spectrophotometer with the KBr pellet technique.

Photocatalytic testing.

Photocatalytic reactions for hydrogen production under natural sunlight were carried out in an air-tight Pyrex tube reactor (irradiation area of 125 cm^2). Photocatalyst samples (0.1 g) were dispersed in 500 mL of an ethanol-water mixture (20 v/v %) in the reactor. The solution was purged with N_2 gas for 30 min before reaction in order to eliminate dissolved oxygen. The volume of gas produced was measured by recording the displacement of water level in an inverted and graduated water-filled burette. The hydrogen gas produced was also confirmed by gas chromatography equipped with TCD detector and carboxen-1010 capillary column.

The photocatalytic hydrogen generation experiments were also performed under visible light irradiation for the purpose of comparison between the samples. The photocatalytic reactions were carried out in a gas-tight 200 ml Pyrex reaction cell at ambient temperature and atmospheric pressure under visible light illumination. In a typical photocatalytic experiment, 20

mg of photocatalysts were dispersed in 70 ml of aqueous solution containing 20 % (v/v) of ethanol. In the case of CdS-Ni and CdS-Pt photocatalyts, $Ni(NO_3)_2$ and H_2PtCl_6 (1.2 wt% of metallic cocatalysts) were also added, respectively. The mixture was evacuated and purged with nitrogen for 30 minutes to remove dissolved oxygen. Then, it was illuminated with a 300W Xe arc lamp equipped with an UV-cutoff filter (≥420 nm) under stirring condition. A 0.5 mL of gas was sampled intermittently through the septum, and hydrogen was analyzed by gas chromatography equipped with TCD detector and carboxen-1010 capillary column.

The apparent quantum yield (QY) was measured under the same photocatalytic reaction conditions. The photon flux was measured with Newport's power meter equipped with a thermopile optical detector.

. The QY was calculated according to following equation:

$$QY\ (\%) = \frac{\text{Number of reacted electron}}{\text{Number of incident photons}} \times 100$$

$$= \frac{\text{Number of evoled } H_2 \text{ molecules } \times\ 2}{\text{Number of incident photons}} \times 100$$

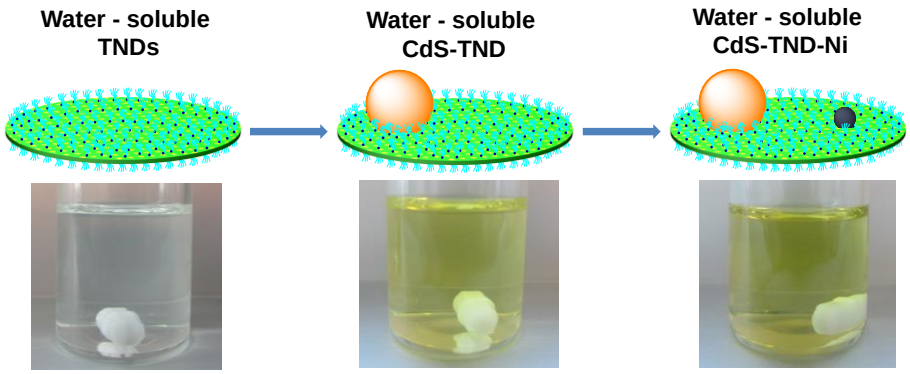

Scheme S1. Schematic illustration of the three steps in the preparation of water-soluble CdS-TND-Ni NCs: (i) synthesis of water-soluble TNDs; (ii) assembly of CdS-TND hybrids; and (iii) formation of water-soluble CdS-TND-Ni NCs.

Table S1. H_2 production rates of reported related CdS based photocatalysts with or without using noble metal cocatalysts

	Photocatalysts	Light source	Sacrificial agent	H_2 generation rate (mmol. h^{-1}. g^{-1})	Refs
Without noble metal cocatalysts	CdS-NiS	Xe-arc 300W, λ≥420 nm	Na_2S + Na_2SO_3	~ 0.600	1
	CdS-$Ni(OH)_2$	Xe-arc 300W, λ≥420 nm	Ethanol	1.461	2
	CdS-$Ni(OH)_2$	Xe-arc 300W, λ≥420 nm	Na_2S + Na_2SO_3	1.556	2
	CdS-NiO	Halogen 500W	Na_2S + Na_2SO_3	0.745	3
	CdS-MoS_2	Xe-arc 300W, λ≥420 nm	Ethanol	~ 0.240	4
	CdS-$KNbO_3$-NiO_x	Hg-Xe 500W, λ≥400 nm	isopropanol	0.150	5
	CdS-Graphene	Xe-arc 200W, λ≥420 nm	Na_2S + Na_2SO_3	0.700	6
	CdS-(N-graphene)	Xe-arc 300W, λ≥420 nm	Na_2S + Na_2SO_3	1.050	7
	CdS-titanate nanosheet	Xe-arc 300W, λ≥420 nm	Na_2S + Na_2SO_3	1.020	8
	CdS-titanate	Xe-arc 800W, λ≥420 nm	Na_2S + Na_2SO_3	~ 0.075	9
	CdS-carbon nanotube	Xe-arc 300W, λ≥400 nm	Na_2S + Na_2SO_3	0.092	10
	CdS-titanate nanotube	Xe-arc 500W, λ≥420 nm	Na_2S + Na_2SO_3	~ 0.450	11
	Water-soluble CdS-TND-Ni	**Xe-arc 300W, λ≥420 nm**	**Ethanol**	**11.038**	This work
	Water-soluble CdS-TND-Ni	**Natural sunlight**	**Ethanol**	**31.820**	This work
With noble metal cocatalysts	CdS-TiO_2-Pt	Hg-arc 500W, λ≥420 nm	Na_2S + Na_2SO_3	~4.00	12
	CdS-ZnO-Pt	Xe-arc 300W	Na_2S + Na_2SO_3	3.870	13
	CdS-(g-C_3N_4)-Pt	Xe-arc 300W, λ≥400 nm	Methanol	0.173	14
	(c-CdS)-Pt-(hex-CdS)	Hg – Xe, λ≥400 nm	isopropanol	0.153	15
	(c-CdS)-Pt-(hex-CdS)	Hg – Xe, λ≥400 nm	Na_2S + Na_2SO_3 + NaOH	0.668	15
	CdS-graphene oxide-Pt	Hg 400W, λ = 365 nm	Methanol	5.500	16
	CdS-titanate nanotube-Pt	Xe-arc 500W, λ≥420 nm	Na_2S + Na_2SO_3	~ 1.750	11
	CdS-carbon nanotube-Pt	Xe-arc 300W, λ≥400 nm	Na_2S + Na_2SO_3	0.819	10
	CdS-ZnO-Au	Xe-arc 300 W	Na_2S + Na_2SO_3	0.608	17
	CdS:Mn-RuO_x	Xe-arc 500W, λ≥420 nm	Na_2S + Na_2SO_3	1.935	18
	ZnO-CdS@Cd-Pt	Xe-arc 300 W	Na_2S + Na_2SO_3	19.200	19

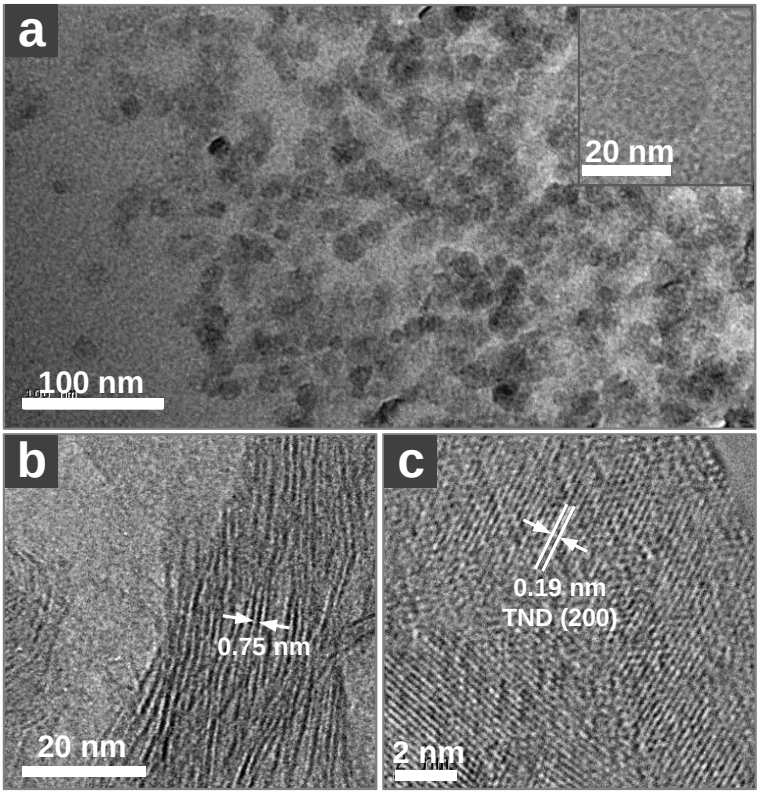

Figure S1. TEM images of the as-synthesized TNDs dispersed in toluene (a), and precipitated in ethanol (b), and HRTEM of TNDs aligned perpendicular to the electron beam (c). Due to the ultrathin structure of TNDs, in the highly dispersed state (i.e. dispersed in toluene), these TNDs tend to lay parallel to the surface of the TEM's grid. Thus, a mean TND's diameter of around 20 nm can be observed (figure a). In the precipitated state (i.e. precipitated in ethanol), some aggregate of TNDs could lay parallel to the direction of the electron beam (figure b), we therefore can calculate the thickness of the TNDs (0.75 nm). Figure c shows a d-spacing of 0.19 nm which is corresponding to the crystalline lattice of (200) plane in the lepidocrocide-type titanate structure.

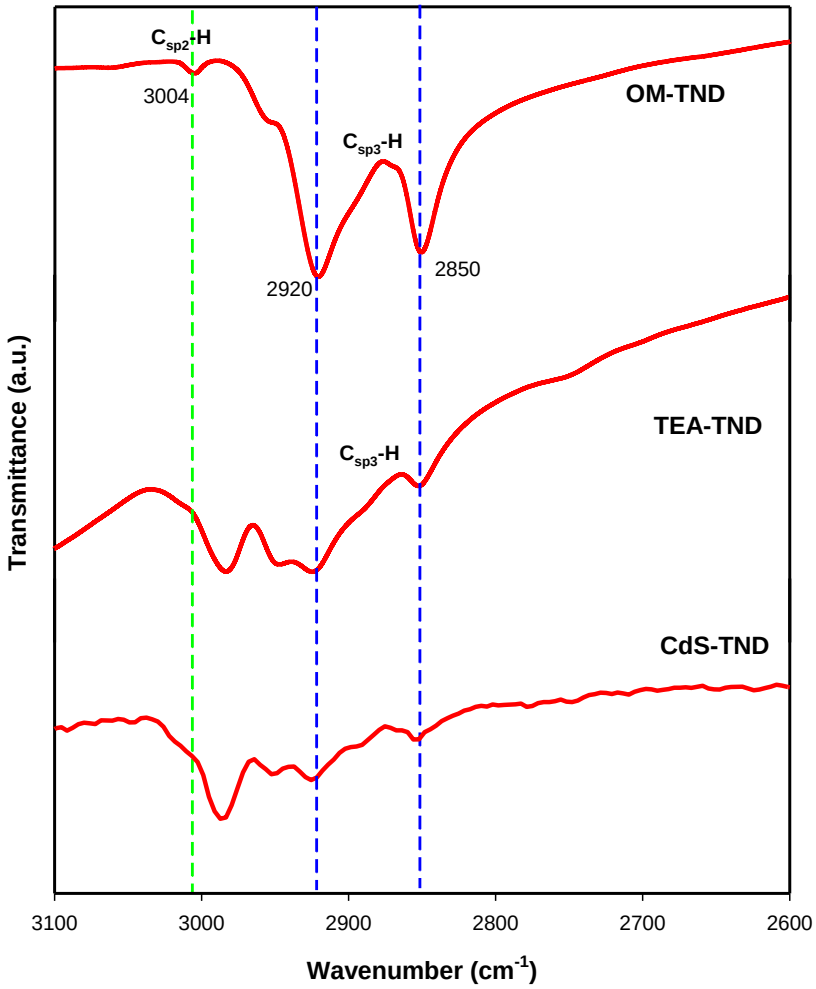

Figure S2. FTIR spectra of as-synthesized OM-TND, TEA-TND obtained by treated OM-TND with TEA, and CdS-TND hybrids. FTIR spectra of all samples show two peaks at 2920 and 2850 cm^{-1} corresponding to the asymmetric and symmetric stretching mode of methylene groups present in the alkyl chain of OM and TEA, respectively. In addition, no absorption at 3004 cm^{-1} which would correspond to the stretching vibration of the C-H bond in the C=C group of OM molecules presents on the FTIR spectrum TEA-TND, indicating that the OM molecules adsorbed on the surface of TNDs have been fully displaced by the TEA cations.

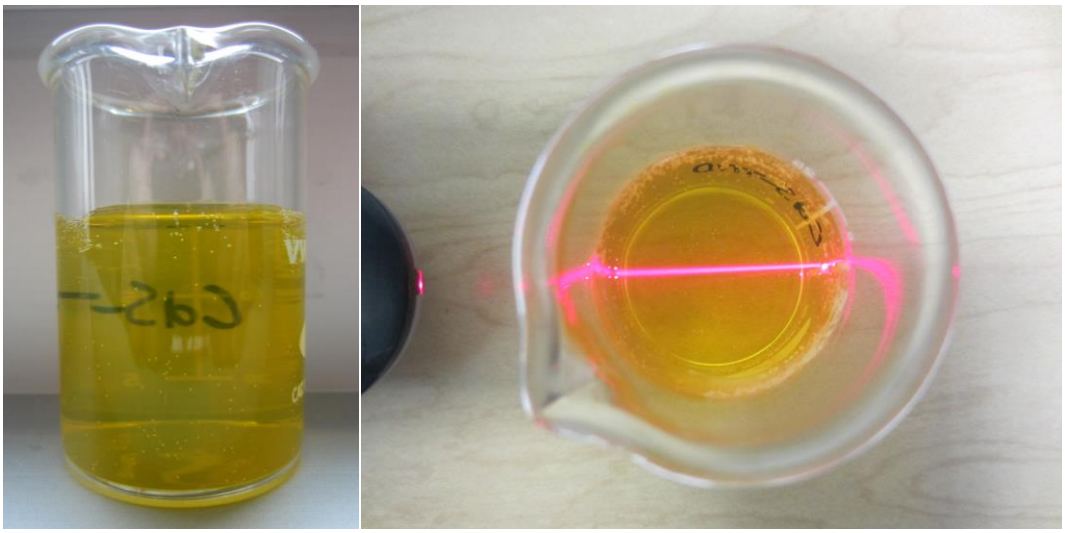

Figure S3. Photo of CdS-TND hybrid colloidal solution showing a clear transparency (left). Photo of CdS-TND solution with a typical Tyndall Effect of colloidal solution.

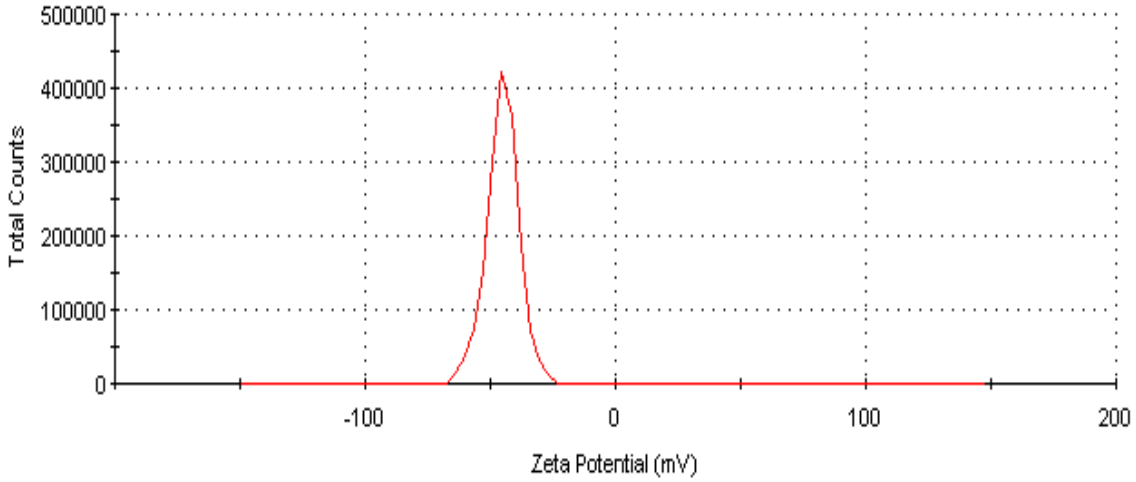

Figure S4. Zeta potential of CdS-TND hybrid colloidal solution measured at pH = 7.5. The CdS-TND solution exhibited a negative zeta potential of 46 mV, indicating a high stability of this colloidal solution. ASTM defines colloids with zeta potentials higher than 40 mV (negative or positive) to have "good stability." [20]

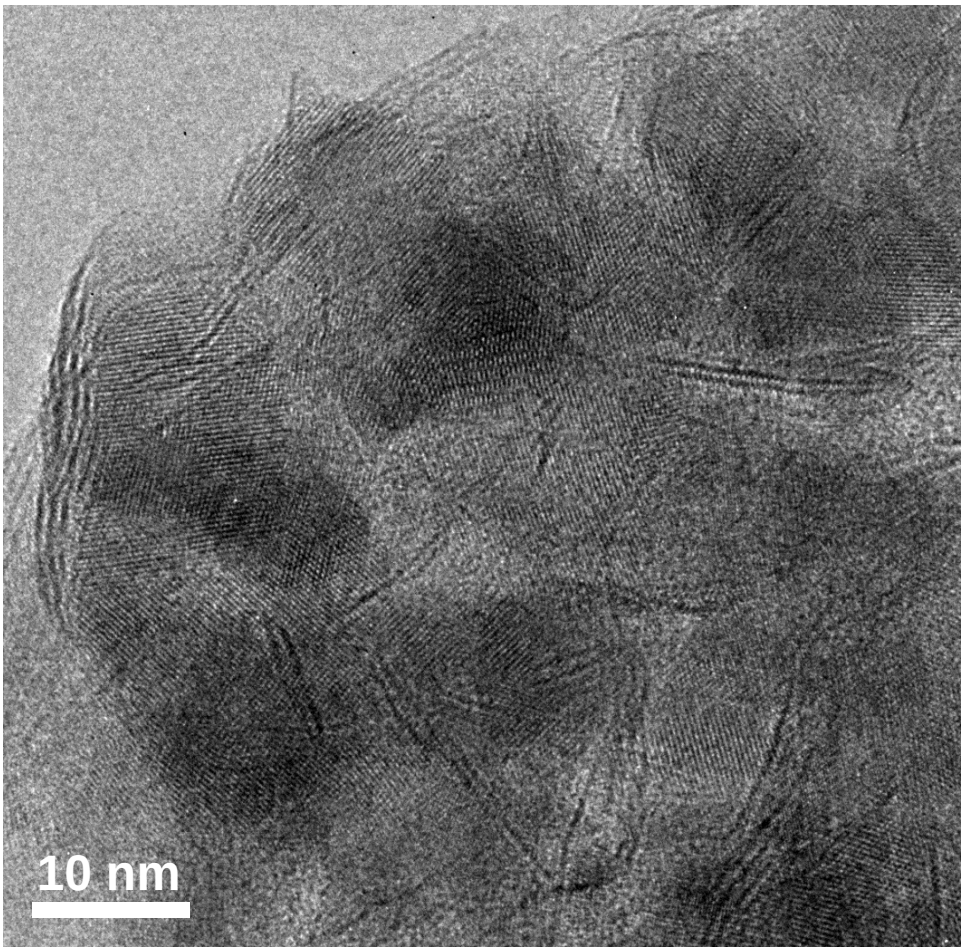

Figure S5. Large area HRTEM image of CdS-TND hybrid obtained by 5 cycles of CdS growth showing the intimate contact between CdS nanoparticles and TNDs

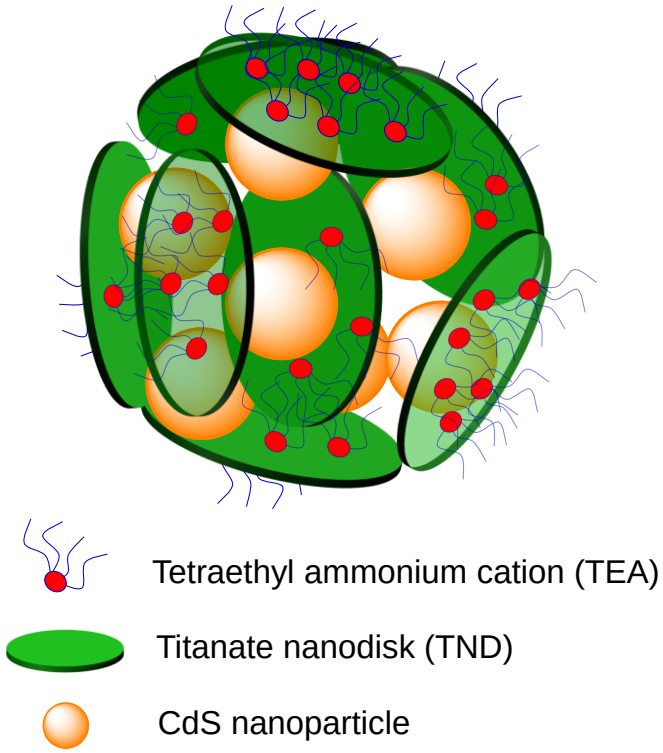

Figure S6. Schematic illustration of the structure of CdS-TND hybrid colloid. Each colloid consists of several TNDs and CdS nanoparticles. The TNDs and CdS nanoparticles are mutually intercalated forming hybrid colloids with multipoint contacts at the interface between the two nano-domains.

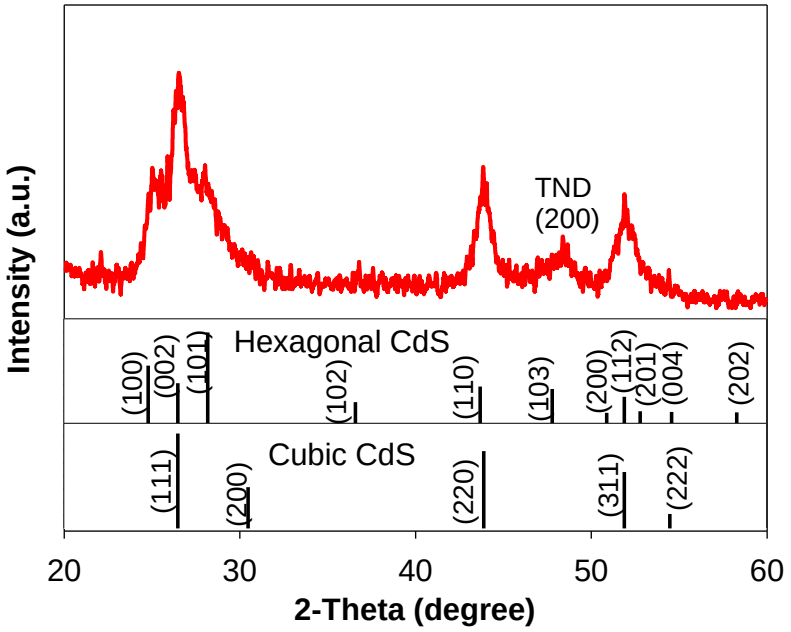

Figure S7. Wide angle powder XRD pattern of the CdS-TND hybrid obtained upon 5 cycles of CdS growth. The standard XRD patterns of cubic and hexagonal CdS are also provided.

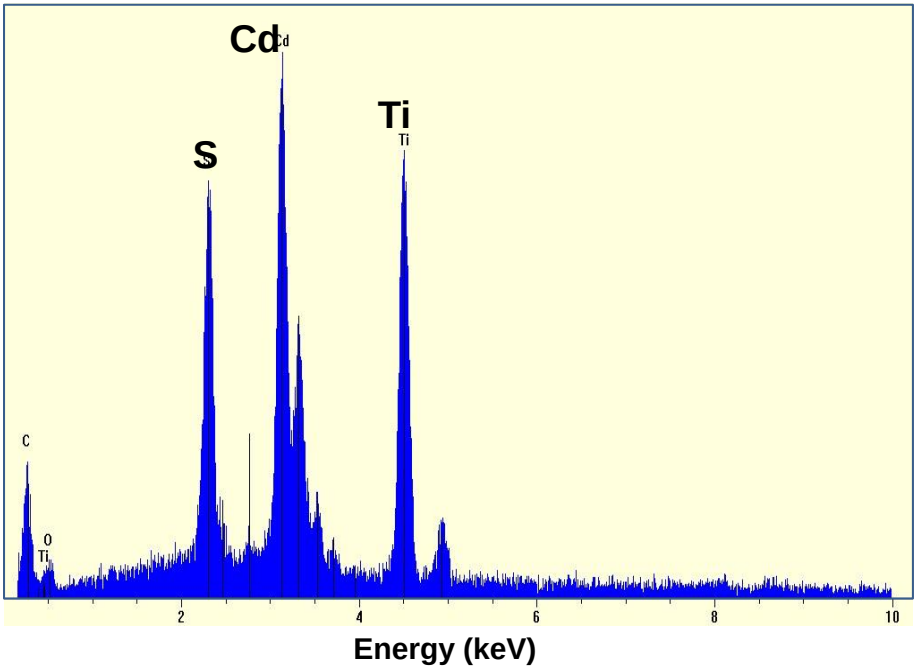

Figure S8. EDX spectrum of CdS-TND hybrids obtained by 5 cycles of CdS growth showing a Cd:Ti molar ratio of 1.14:1.

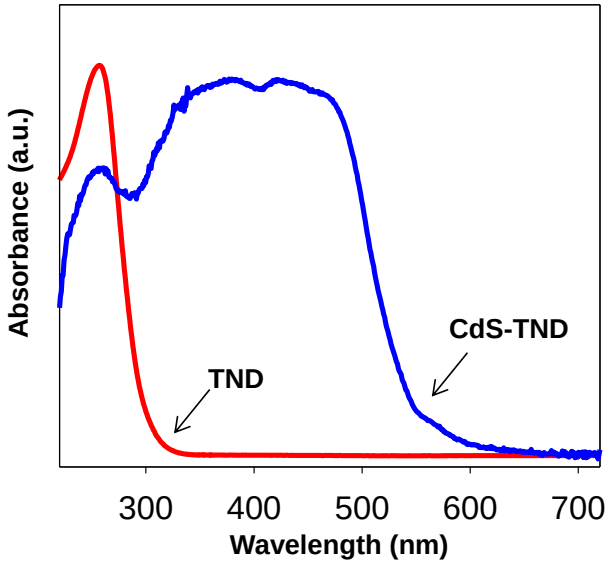

Figure S9. UV-vis diffusive reflectance spectra of the CdS-TND hybrids in comparison to that of TNDs.

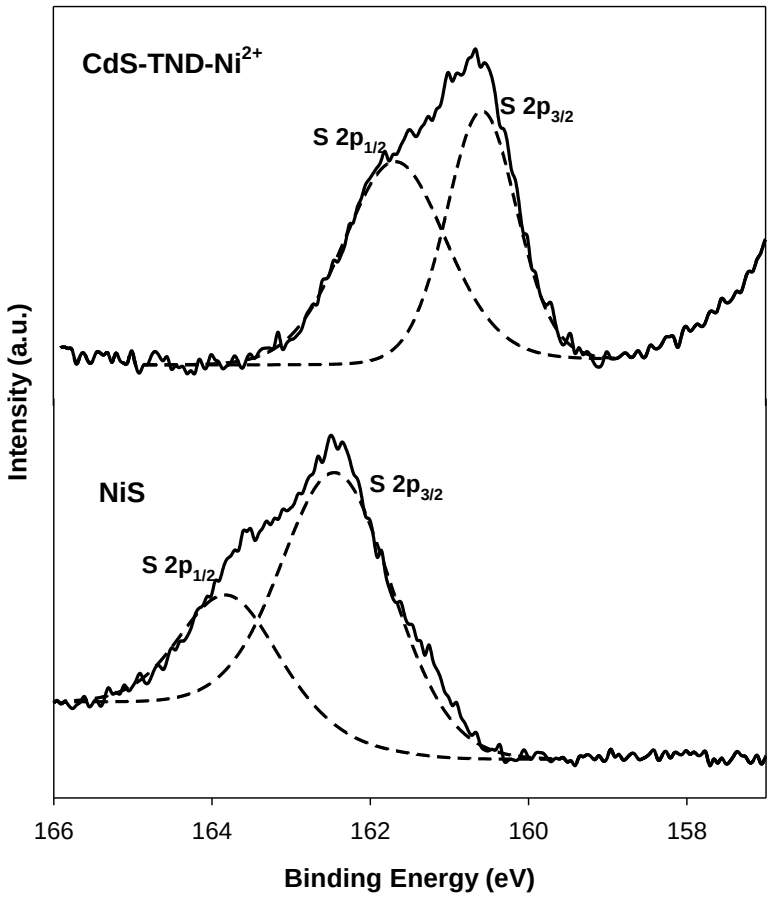

Figure S10. XPS spectrum of S 2p in the CdS-TND-Ni^{2+} in comparison to that of S 2p in NiS prepared by reacting Ni^{2+} with Na_2S. It is observed that, the S 2p XPS spectrum of CdS-TND-Ni^{2+} shows two peaks at 160.5 and 161.6 eV, corresponding to the binding energy of S $2p_{3//2}$ and S $2p_{1/2}$, respectively.[21] No peaks at 162.3 and 163.7 eV in the S 2p XPS spectrum of NiS[22] was observed in the S 2p XPS spectrum of CdS-TND-Ni^{2+}, indicating the absence of NiS in the CdS-TND-Ni^{2+}.

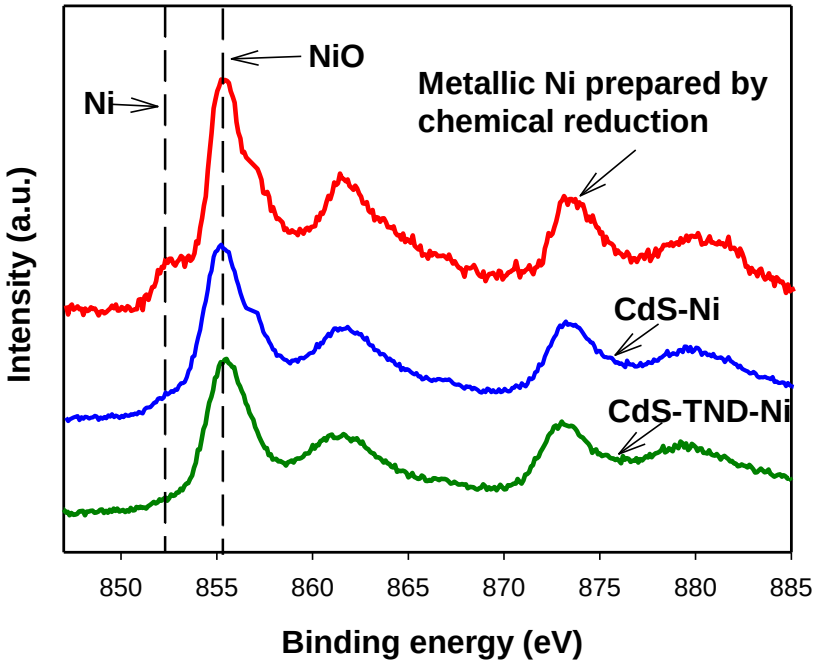

Figure S11. XPS spectrum of Ni 2p in the CdS-TND-Ni NCs in comparison to those of Ni in CdS-Ni obtained by photoreduction of Ni^{2+} on CdS, and metallic Ni nanoparticles prepared by chemical reduction using $NaBH_4$ as reducing agent and $Ni(NO_3)_2$ as nickel precursor.

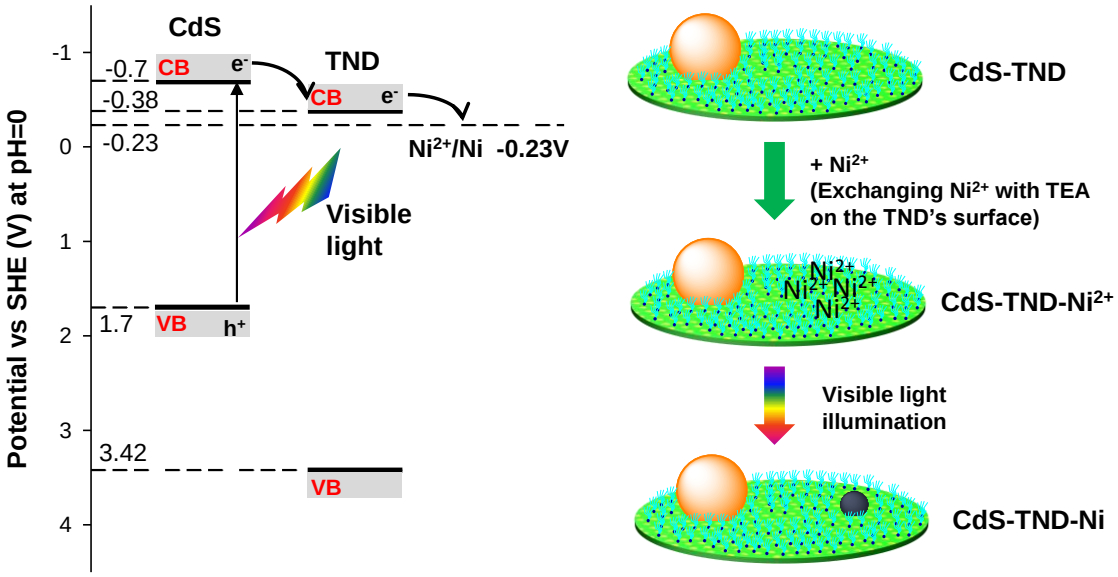

Figure S12. Schematic illustration of the electron transfer in the photoreduction of Ni^{2+} adsorbed on the surface of TNDs under visible light illumination (left). Schematic illustration of the formation of Ni clusters on the surface of TND in the CdS-TND hybrids by visible light illumination (right).

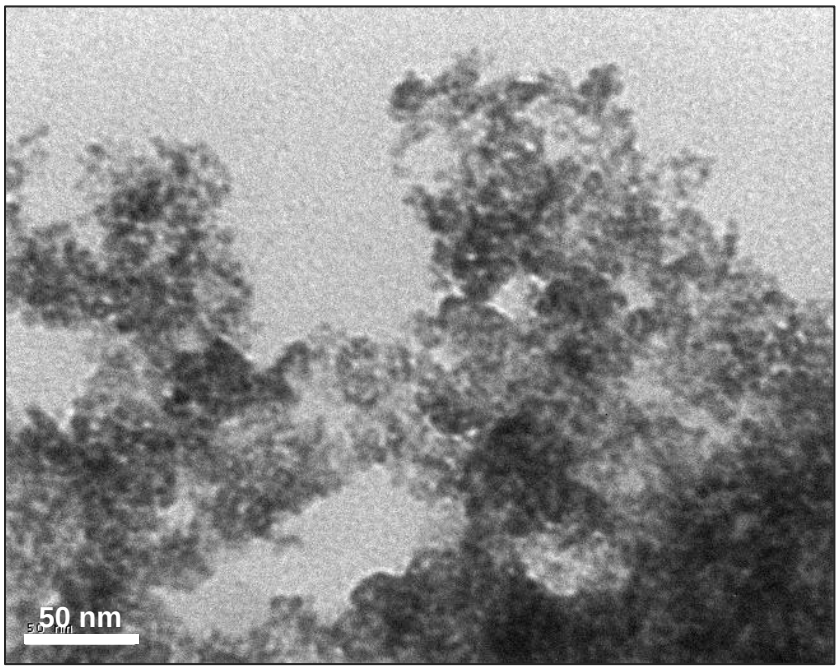

Figure S13. TEM image of CdS nanoparticles obtained under similar conditions to those of CdS-TND hybrids, except for the absence of TNDs. It can be seen that, the size of the CdS nanoparticles are around 6 nm which are similar to those of CdS nanoparticles in the CdS-TND-Ni nanocomposites. These CdS nanoparticles are aggregated forming large precipitate.

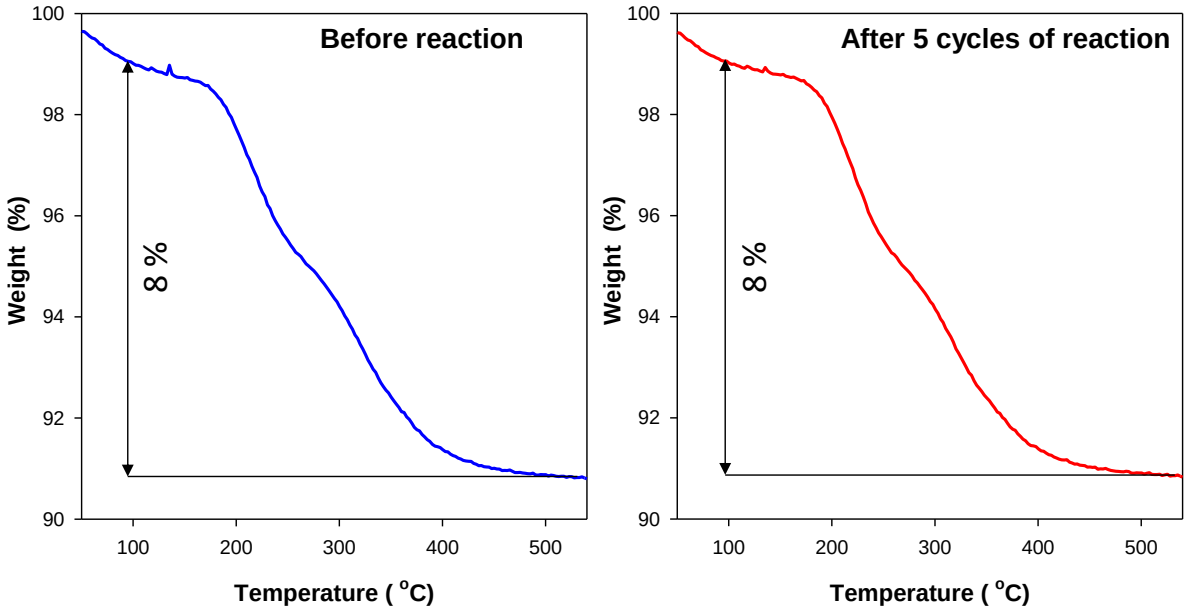

Figure S14. TGA curves of CdS-TND-Ni NCs before and after 5 cycles of hydrogen generation reaction.

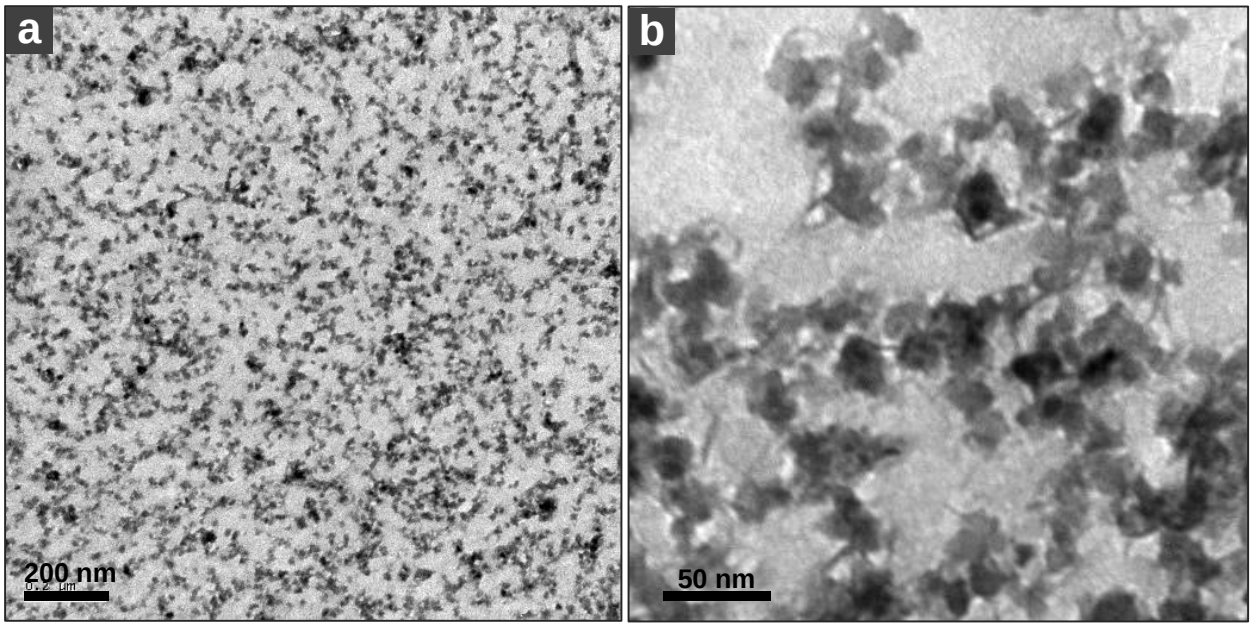

Figure S15. Low magnification (a) and high magnification (b) TEM images of CdS-TND-Ni nanocomposites after 5 cycles (15 h) of reaction. The low magnification image shows that the photocatalysts are still highly dispersed in solution after the reaction. The high magnification image reveals that the morphology of the CdS-TND-Ni nanocomposites is preserved after 5 cycles.

References

1. Chen, X.; Chen, W.; Lin, P.; Yang, Y.; Gao, H.; Yuan, J.; Shangguan, W. *Catal. Commun.* **2013**, *36*, 104.
2. Ran, J.; Yu, Y. G.; Jaroniec, M. *Green Chem.* **2011**, *13*, 2708.
3. Khan, Z.; Khannam, M.; Vinothkumar, N.; De, M.; Qureshi, O. *J. Mater. Chem.* **2012**, *22*, 12090.
4. Zong, X.; Wu, G.; Yan, H.; Ma, G.; Shi, J.; Wen, F.; Wang, L.; Li, C. *J. Phys. Chem. C* **2010**, *114*, 1963.
5. Choi, J.; Ryu, S. Y.; Balcerski, W.; Lee, T. K.; Hoffmann, M. R. *J. Mater. Chem.* **2008**, *18*, 2371.
6. Ye, A.; Fan, W.; Zhang, Q.; Deng, W.; Wang, Y. *Catal. Sci. Technol.* **2012**, *2*, 969.
7. Jia, L.; Wang, D. H.; Huang, Y. X.; Xu, A. W.; Yu, H. Q. *J. Phys. Chem. C* **2011**, *115*, 11466.
8. Kim, H. N.; Kim, T. W.; Kim, I. Y.; Hwang, S. J. *Adv. Funct. Mater.* **2011**, *21*, 3111.
9. Zhang, Y.; Tang, Y.; Liu, X.; Dong, Z.; Hng, H. H.; Chen, Z.; Sum, T. C.; Chen, X. *Small* **2013**, *9*, 996.
10. Kim, Y. K.; Park, H. *Energy Environ. Sci.* **2011**, *4*, 685.
11. Chen, Y.; Wang, L.; Lu, G. M.; Yao, X.; Guo, L. *J. Mater. Chem.* **2011**, *21*, 5134.
12. Jang, J. S.; Choi, S. H.; Kim, H. G.; Lee, J. S. *J. Phys. Chem. C* **2008**, *112*, 17200.
13. Wang, X.; Liu, G.; Chen, Z. G.; Li, F.; Wang, L.; Lu, G. Q.; Cheng, H. M. *Chem. Commun.* **2009**, 3452.
14. Ge, L.; Zuo, F.; Liu, J.; Ma, Q.; Wang, C.; Sun, D.; Bartels, L.; Feng, P. *J. Phys. Chem. C* **2012**, *116*, 13708.
15. Silva, L. A.; Ryu, S. Y.; Choi, J.; Choi, W.; Hoffmann, M. R. *J. Phys. Chem. C* **2008**, *112*, 12069.
16. Gao, P.; Liu, J.; Lee, S.; Zhang, T.; Sun, D. D. *J. Mater. Chem.* **2012**, *22*, 2292.
17. Yu, Z. B.; Xie, Y. P.; Liu, G.; Lu, G. Q. M.; Ma, X. L.; Cheng, H. M. *J. Mater. Chem. A*, **2013**, *1*, 2773.
18. Ikeue, K.; Shiiba, S.; Machida, M. *Chem. Mater.* **2010**, *22*, 743.
19. Wang, X.; Liu, G.; Wang, L.; Chen, Z. G.; Lu, G, Q, M.; Cheng, H. M. *Adv. Energy Mater.* **2012**, *2*, 42.

20. *Zeta Potential of Colloids in Water and Waste Water*, ASTM Standard D 4187 - 82, American Society for Testing and Materials, 1985.
21. Bhide, V.G.; Salkalachen, S.; Rastog, A.C.; Rao, C.N.R.; Hegde, M.S. *J. Phys. D: Appl. Phys.* **1981**, *14*, 1647.
22. Shalvoy, R.B.; Reucroft, P.J. *J. Vac. Sci. Technol.* **1979**, *16*, 567.